EPJ Web of Conferences **206**, 05001 (2019) https://doi.org/10.1051/epjconf/201920605001
ISMD 2018

Recent NA48/2 results on rare kaon decays

Dmitry Madigozhin[1,*]

[1]Joint Institute for Nuclear Research, Joliot-Curie, 6, Dubna, Moscow region 141980, Russia
e-mail: madigo@cern.ch.

Abstract. NA48/2 results contributing to ChPT testing are presented. A sample of 1663 events of the rare decay $K^{\pm} \to \mu^{\pm}\nu e^{+}e^{-}$ has been selected with a minimum $e^{+}e^{-}$ effective mass of 140 MeV. The measured model independent decay rate is in agreement with ChPT predictions. The branching ratio of the $K^{\pm} \to \pi^{\pm}\pi^{0}e^{+}e^{-}$ decay, never observed so far, has been obtained from a sample of about 5000 candidates with less than 6% background, also in agreement with ChPT predictions. In addition, a most precise measurement of the charged kaon semileptonic form factors has been obtained from 4.4 million K_{e3} and 2.3 million $K_{\mu 3}$ events collected in 2004.

1 The NA48/2 beam and detector

The NA48/2 experiment at the CERN SPS was designed to search for direct CP violation in $K^{\pm}$ decays to three pions [1]. The detector and beam of the experiment are described in details in [1, 2]. Two simultaneous beams of charged particles containing nearly 6% of $K^{\pm}$ were produced by 400 GeV/c protons impinging on a beryllium target (see Fig. 1). Particles of opposite charge with a central momentum of 60 GeV/c and a momentum band of ±3.8% (*rms*) were selected by a system of magnets and collimators. Two resulting beams, each $\approx$ 1 cm wide, were superimposed in the decay volume inside a 114 m long vacuum tank.

Tracks of the charged particles from $K^{\pm}$ decays were measured by a magnetic spectrometer consisting of four drift chambers (DCH1–DCH4) and a dipole magnet located between the second and third chamber. Each chamber consisted of four staggered double planes of sense wires measuring the coordinates transverse to the beam axis along the 0°, 90° and ± 45°

*for the NA48/2 Collaboration: G. Anzivino, R. Arcidiacono, W. Baldini, S. Balev, J.R. Batley, M. Behler, S. Bifani, C. Biino, A. Bizzeti, B. Bloch-Devaux, G. Bocquet, N. Cabibbo, M. Calvetti, N. Cartiglia, A. Ceccucci, E. Celeghini, P. Cenci, C. Cerri, C. Cheshkov, J.B. Chèze, M. Clemencic, G. Collazuol, F. Costantini, A. Cotta Ramusino, D. Coward, D. Cundy, A. Dabrowski, P. Dalpiaz, C. Damiani, M. De Beer, J. Derré, H. Dibon, L. DiLella, N. Doble, K. Eppard, V. Falaleev, R. Fantechi, M. Fidecaro, L. Fiorini, M. Fiorini, T. Fonseca Martin, P.L. Frabetti, L. Gatignon, E. Gersabeck, A. Gianoli, S. Giudici, A. Gonidec, E. Goudzovski, S. Goy Lopez, M. Hita-Hochgesand, M. Holder, P. Hristov, E. Iacopini, E. Imbergamo, M. Jeitler, G. Kalmus, V. Kekelidze, K. Kleinknecht, V. Kozhuharov, W. Kubischta, G. Lamanna, C. Lazzeroni, M. Lenti, L. Litov, D. Madigozhin, A. Maier, I. Mannelli, F. Marchetto, R. Marchevski, G. Marel, M. Markytan, P. Marouelli, M. Martini, L. Masetti, E. Mazzucato, A. Michetti, I. Mikulec, M. Misheva, N. Molokanova, E. Monnier, U. Moosbrugger, C. Morales Morales, D.J. Munday, A. Nappi, G. Neuhofer, A. Norton, M. Patel, M. Pepe, A. Peters, F. Petrucci, M.C. Petrucci, B. Peyaud, M. Piccini, G. Pierazzini, I. Polenkevich, Yu. Potrebenikov, M. Raggi, B. Renk, P. Rubin, G. Ruggiero, M. Savrié, M. Scarpa, M. Shieh, S. Shkarovskiy, M.W. Slater, M. Sozzi, S. Stoynev, E. Swallow, M. Szleper, M. Valdata-Nappi, B. Vallage, M. Velasco, M. Veltri, S. Venditti, M. Wache, H. Wahl, A. Walker, R. Wanke, L. Widhalm, A. Winhart, R. Winston, M.D. Wood, S.A. Wotton, A. Zinchenko, M. Ziolkowski.

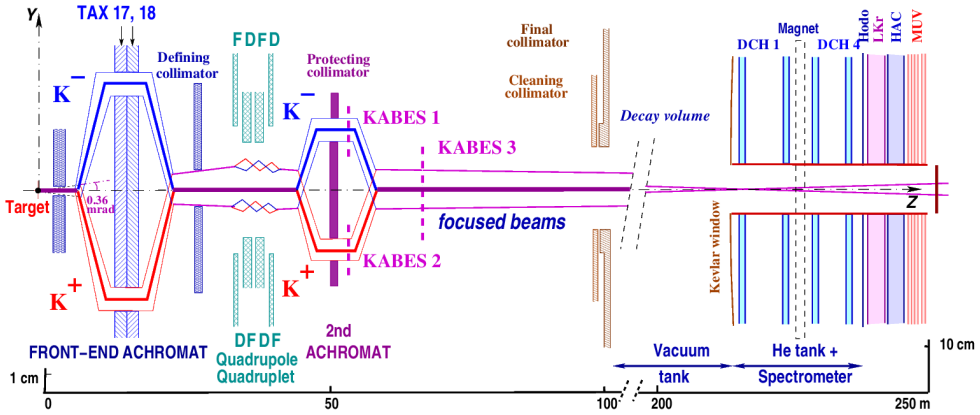

Figure 1. Sketch of the NA48/2 beam line, decay volume and detectors

directions. The spectrometer was located in a tank filled with helium at nearly atmospheric pressure.

The spatial resolution of each chamber was ~90 μm, and the momentum resolution was $\sigma_p/p = (1.02 \oplus 0.044 \cdot p)\%$ (momentum p in Gev/c). The spectrometer was followed by a scintillator hodoscope (HOD) with a time resolution of ~150 ps, whose signals were used to trigger the readout of events with at least one charged track

A liquid krypton calorimeter (LKr) was located behind the hodoscope and used to measure the position and energy of electrons and photons. It is an approximately homogeneous ionization chamber with an active volume of 7 m^3 of liquid krypton, 27 X_0 deep, segmented transversally into 13248 projective cells, 2×2 cm^2 each. The transverse position of isolated showers was measured with a spatial resolution $\sigma_x = \sigma_y = (0.42/\sqrt{E} \oplus 0.06)$ cm. Energy resolution for photons and electrons was $\sigma_E/E = (3.2/\sqrt{E} \oplus 9.0/E \oplus 0.42)\%$ (energy E in GeV). Another hodoscope (NHOD) consisting of a plane of scintillating fibers, was located inside the LKr calorimeter for triggering purposes.

The LKr was followed by a hadronic calorimeter with a total iron thickness of 1.2 m. The muon system MUV, consisting of three scintillator planes and 80 cm thick iron walls, was used for muon identification. A 15.8 cm diameter evacuated aluminium tube of 1.1 mm thickness traversing the centre of the main detectors allowed the undecayed beam particles and the muon halo from beam pion decays to continue their path in vacuum.

2 Study of the $K^\pm \to \mu^\pm \nu e^+ e^-$ decay

The radiative leptonic decay $K^\pm \to \mu^\pm \nu \gamma^* (\gamma^* \to e^+ e^-)$ proceeds via two different mechanisms. The main contribution is the Inner Bremsstrahlung (IB) from the final state muon, that can be calculated from QED. The virtual γ^* can also be radiated off at the weak vertex of the intermediate state. This Structure Dependent (SD) contribution depends on the form factors that can be calculated in the framework of ChPT and becomes dominant at large e^+e^- mass values $M_{ee} > 140$ MeV/c^2. This is the most interesting region of the decay phase space with a small contribution to the total branching ratio. Therefore a large amount of kaon decays is needed to make a precision measurement in this part of the phase space.

The analysis is based on the reconstruction of three-track vertices. One of the tracks is required to be identified as a muon according to LKr and MUV information, while the two

others are to be identified as an electron and a positron using LKr and DCH. The abundant $K^{\pm} \to \pi^{\pm}\pi^{+}\pi^{-}$ ($K_{3\pi}$) decay is used for normalization. Reconstructed momenta of selected tracks are required to be in the range (3–50) GeV/c, and the total vertex momentum to be < 66 GeV/c.

The requirement $M_{ee} > 140$ MeV/c^2 suppresses background from decay chains with a π^0 Dalitz decay to $e^+e^-\gamma$, while requiring the muon-neutrino invariant mass $M_{\mu\nu} > 170$ MeV/c^2 suppresses background from $K^{\pm} \to \pi^{\pm}e^+e^-$ followed by $\pi^{\pm} \to \mu^{\pm}\nu$ decay.

The particle identification is based on LKr and MUV. The minimum distance between the different electromagnetic showers in LKr associated with the charged tracks have to be at least 20 cm to avoid showers overlapping effects. The ratio E_{LKr}/P_{DCH} of the energy deposit in LKr E_{LKr} and the momentum measured by the spectrometer P_{DCH} is used to distinguish muons, pions and electrons. Muon is required to have $E_{LKr}/P_{DCH} < 0.2$ and an assiciated MUV signal. For electrons we require $0.95 < E_{LKr}/P_{DCH} < 1.05$ and a linear discriminant variable which makes use of the different shape and depth of the created showers. This discriminant provides almost complete suppression of pions from $K_{3\pi}$ and $K^{\pm} \to \pi^{+}\pi^{-}e^{\pm}\nu_e$ decays.

The residual background comes from $K^{\pm} \to \pi^{\pm}\pi^{+}\pi^{-}$ and $K^{\pm} \to \pi^{+}\pi^{-}e^{\pm}\nu$ decays followed by a pion decay and/or pion misidentification and from $K^{\pm} \to \pi^{\pm}\pi^0\pi^0$ followed by the Dalitz decay $\pi^0 \to e^+e^-\gamma$ (π^0_D) of both neutral pions. The total background is evaluated from the selected Wrong Sign events (containing a reconstructed same sign e^+e^+ or e^-e^- pair forbidden in Standard Model), coming from the above sources with a scaling factor defined by the possible charge combinations.

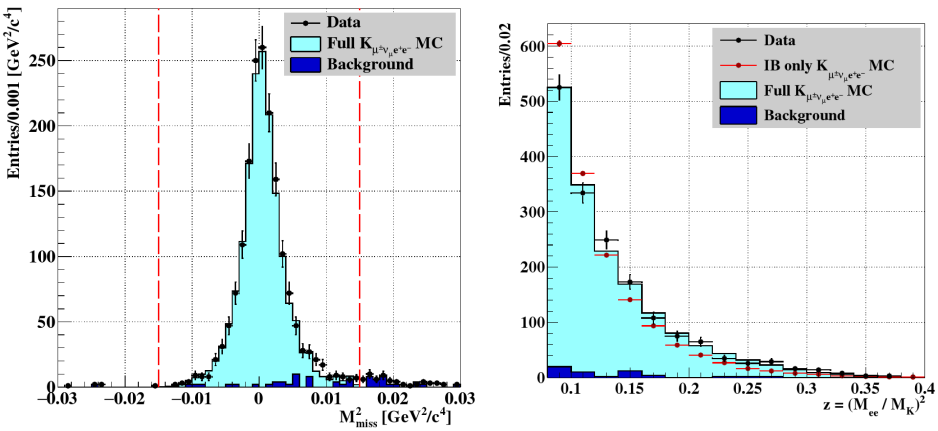

Figure 2. Left plot: missing mass squared distribution after the final selection. Vertical lines show the signal region. Right plot: z distribution after the final selection. The results of signal MC simulation for the full MC model and for the IB contribution only are scaled to the total number of experimental events after background subtraction.

A sample of 1663 signal candidates is selected with an estimated background of 54 ± 11 events in an exposure to 1.56×10^{11} kaon decays in 2003–2004 (see Fig.2 left plot for the missing mass spectrum). The spectrum of the variable $z = (M_{ee}/M_K)^2$ shown in the right plot of the Fig.2 is compatible with the prediction of ChPT [4]. The signal simulation result obtained only with the IB contribution demonstrates that the data are clearly more compatible with ChPT calculation.

The partial branching ratio is computed in each bin of z and includes radiative corrections as implemented using the PHOTOS package. The sum of these contributions represent a model-independent branching ratio for $M_{ee} > 140$ MeV/c^2 : $BR(K^\pm \to \mu^\pm \nu e^+ e^-) = (7.84 \pm 0.21_{stat} \pm 0.08_{syst} \pm 0.06_{ext}) \times 10^{-8}$. The systematic uncertainty is dominated by the contributions related to radiative corrections and background while the external error is due to the normalization branching ratio uncertainty [3].

The result is compatible with the theoretical prediction [4] and with the earlier measurements [5, 6]. It is the first measurement of this mode performed with the radiative corrections taken into account. The resulting uncertainty of the measured branching ratio is improved by the factor of 1.5 with respect to the most precise previous measurement [5].

3 First observation of the $K^\pm \to \pi^+\pi^0 e^+ e^-$ decay

The radiative decay $K^\pm \to \pi^+\pi^0 e^+ e^-$ proceeds via a similar mechanisms, $K^\pm \to \pi^+\pi^0\gamma^*(\gamma^* \to e^+e^-)$ as the previous one and has not been observed so far. The signal events are selected concurrently with the normalization events $K^\pm \to \pi^\pm\pi^0$ followed by neutral pion Dalitz decay $\pi^0 \to \gamma e^+ e^-$ (π^0_D).

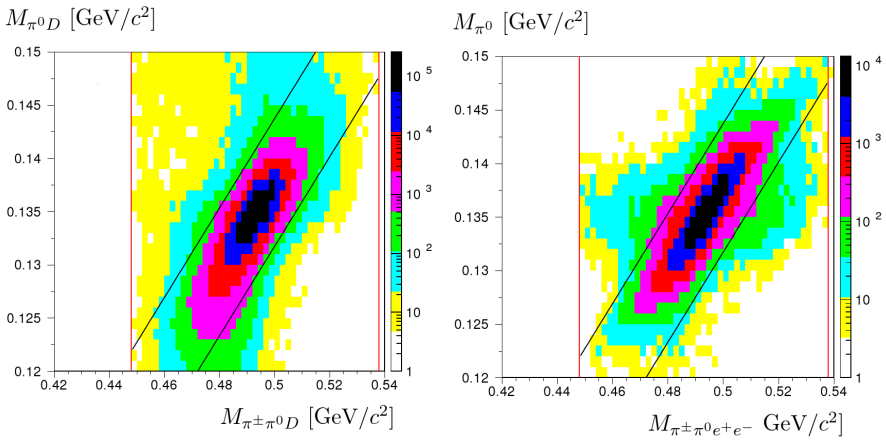

Figure 3. Left plot: normalization simulated candidates in the plane of reconstructed masses ($M_{\pi^\pm\pi^0 D}$,$M_{\pi^0 D}$). Right plot: signal simulated candidates in the plane of reconstructed masses ($M_{\pi^\pm\pi^0 e^+e^-}$,M_{π^0}). The vertical lines and the slanted bands correspond to the selection constraints.

Both signal and normalization candidates are reconstructed from three-track vertices with the track reconstructed momenta in the range (2–60) GeV/c. The tracks are required to be in time within 5 ns of each other using the HOD time associated to each of the considered tracks. The radial distance between the track and the beam axis monitored by fully reconstructed $K^\pm \to \pi^\pm\pi^+\pi^-$ decays should be larger than 12 cm in all the drift chambers. Any track-to track distance at DCH1 should be larger than 2 cm to suppress photons conversions to an e^+e^- pair in the upstream material. Events with all three tracks hitting the same HOD quadrant are rejected for trigger efficiency.

Energy clusters in LKr without associated track, in time within 5 ns with the vertex time are identified as the photon candidates. The minimum photon energy should be 2 GeV. The photon momenta are reconstructed assuming the decay position defined by the 3-track vertex.

The two-photon invariant mass of a signal events ($\gamma e^+ e^-$ for normalization events) is required to be within ± 15 MeV/c^2 from the π^0 PDG mass [3], and the reconstructed kaon

mass to be within ±45 MeV/c^2 from the $K^\pm$ PDG mass. The total momentum is required to be in the range (54–66) GeV/c.

The correlation between the reconstructed π^0 and kaon masses defines a kinematic constraint $|M_{\pi^0} - 0.42M_K + 73.2| < 6$ MeV/c^2 (see Fig. 3) allowing particle identification without using E_{LKr}/P_{DCH} requirements, therefore increasing acceptance of low momentum tracks.

The two main background sources are $K^\pm \to \pi^\pm\pi^0\pi^0_D$ (with a lost photon) and $K^\pm \to \pi^\pm\pi^0_D$ (with an extra accidental photon combined with the Dalitz decay photon leading to imitation of a $\pi^0 \to \gamma\gamma$ decay). The first background is additionally suppressed by requiring the squared invariant mass of the $\pi^\pm\pi^0$ system to be larger than 0.12 GeV^2/c^4. To reject further the second background source, the both possible invariant masses $M_{ee\gamma}$ are required to be more than 7 MeV/c^2 away from the π^0 PDG mass. The 0.15% background to normalization is due to $K^\pm \to \mu^\pm\nu\pi^0_D$ and $K^\pm \to e^\pm\nu\pi^0_D$ misreconstructed events where the pion mass is assigned to the lepton candidate.

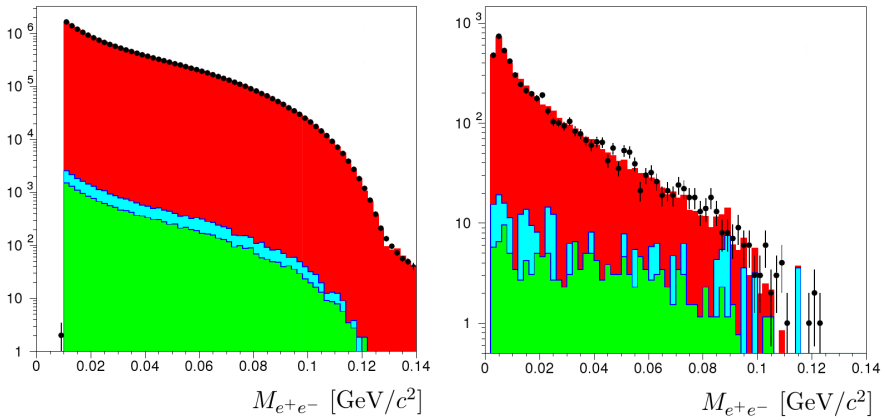

Figure 4. Reconstructed e^+e^- invariant mass distributions for the normalization $\pi^\pm\pi^0 D$ candidates (left) and for the signal $\pi^\pm\pi^0e^+e^-$ events (right). Full dots correspond to data candidates. Stacked histograms on the left plot are, from bottom to top, the expected $K_{\mu 3D}$ and K_{e3D} backgrounds and the normalization distribution. Stacked histograms on the right plot are, from bottom to top, the expected $K_{3\pi D}$ and $K_{2\pi D}$ backgrounds and the signal IB simulation result.

Samples of 5076 signal candidates and 16.8×10^6 normalization $K_{2\pi D}$ candidates have been selected from an exposure to 1.7×10^{11} kaon decays in 2003–2004. The background contamination estimated from simulation is about 5.7% in the signal mode and 0.15% in the normalization mode. Reconstructed e^+e^- invariant mass distributions for the normalization and signal candidates are shown in the Fig. 4. Expected background, normalization and signal histograms, normalized to the number of observed candidates, show a good agreement with the data distributions.

The preliminary result for the branching ratio is $BR(K^\pm \to \pi^+\pi^0e^+e^-) = (4.22 \pm 0.06_{stat} \pm 0.04_{syst} \pm 0.13_{ext}) \times 10^{-6}$, where the systematic error includes uncertainties related to acceptances, trigger efficiencies and radiative corrections. The external error is due to the normalization mode branching ratio uncertainty [3]. The obtained result is in agreement with the theoretical prediction [7] of 4.10×10^{-6} (obtained including isospin corrections but without radiative corrections).

4 Measurement of the $K^{\pm}_{l3}$ form factors

In the approximation of negligible electromagnetic effects, the $K_{l3}(l = \mu, e)$ differential rate as a function of the lepton and pion energies in the kaon rest frame (Dalitz plot) may be parameterised [8] in terms of the vector $f_+(t)$ and scalar $f_0(t)$ form factor functions of $t = (P_K - P_\pi)^2$:

$$\frac{d^2\,\Gamma(K^{\pm}_{l3})}{dE^*_l\,dE^*_\pi} = \rho(E^*_l, E^*_\pi) \propto \left(A_1\,|f_+(t)|^2 + A_2\,f_+(t)f_-(t) + A_3\,|f_-(t)|^2\right), \tag{1}$$

where E^*_l and E^*_π are the lepton and pion energies in the kaon rest frame; $f_-(t) = (f_0(t) - f_+(t))(m^2_K - m^2_{\pi^0})/t$; m_K and m_{π^0} are the charged kaon and neutral pion masses [3]. The K_{l3} form factors participate in the determination of the $|V_{us}|$ CKM matrix element [9] trough the phase space integrals of the differential rates. The kinematic factors are

$$\begin{aligned} A_1 &= m_K\left(2\,E^*_l\,E^*_\nu - m_K(E^{*,\max}_\pi - E^*_\pi)\right) + m^2_l\,((E^{*,\max}_\pi - E^*_\pi)/4 - E^*_\nu), \\ A_2 &= m^2_l\,(E^*_\nu - (E^{*,\max}_\pi - E^*_\pi)/2), \\ A_3 &= m^2_l\,(E^{*,\max}_\pi - E^*_\pi)/4. \end{aligned} \tag{2}$$

Here $E^{*,\max}_\pi = (m^2_K + m^2_{\pi^0} - m^2_l)/2\,m_K$, m_l is the charged lepton mass, and $E^*_\nu = m_K - E^*_l - E^*_\pi$ is the neutrino energy in the kaon rest frame. In the case of K_{e3} decay, the scalar form factor terms become negligible due to the small electron mass.

Recently, a measurement of the form factor parameters has been performed by the NA48/2 Collaboration [11] for K_{e3} and $K_{\mu3}$ decay modes. Results of the joint K_{l3} analysis from the paper are presented here. Three K_{l3} form factor parameterizations were used:

- Taylor expansion [3] ($f_+(t) = 1 + \lambda'_+ t/m^2_\pi + \frac{1}{2}\lambda''_+(t/m^2_\pi)^2$, $f_0(t) = 1 + \lambda'_0 t/m^2_\pi$),
- Pole [10] ($f_+(t) = \frac{M^2_V}{(M^2_V - t)}$, $f_0(t) = \frac{M^2_S}{(M^2_S - t)}$),
- Dispersive [12] ($f_+(t) = \exp\left(\frac{(\Lambda_+ + H(t))t}{m^2_\pi}\right)$, $f_0(t) = \exp\left(\frac{(ln[C] - G(t))t}{(m^2_K - m^2_\pi)}\right)$),

where m_π is the mass of charged pion. The external functions $H(t), G(t)$ of the Dispersive parameterization depend on five extra parameters, that are fixed with some precision from other experimental data and theoretical considerations [12].

For the semileptonic decays reconstruction and selection, LKr energy clusters and charged particle tracks are reconstructed as described in [1]. An event is considered as a K_{l3} candidate, if there is at least 2 LKr clusters consistent with photons of reconstructed energy above 3 GeV, and the sum of their energies is above 15 GeV, ensuring high trigger efficiency. The distances between the selected cluster and impact points at the LKr front plane of each in-time (within ±10 ns) track should be larger than 15 cm. Photon candidates are required to be at least 8 cm away from the LKr edges. The decay vertex longitudinal position Z_n is reconstructed from the photon energies and positions at LKr under the assumption that they are produced in the decay of a π^0 of PDG mass value [3].

At least one charged track is required with a minimum momentum of 5 GeV/c (10 GeV/c) for the $K_{e3}(K_{\mu3})$ selection. Tracks with $E_{LKr}/P_{DCH} > 0.9$ are identified as electrons (positrons), otherwise the muon identification hypothesis was tested using MUV information. The transverse position of the decay vertex is defined by the track coordinates at Z_n. A wide Z_n-dependent cut is applied to the distance between the vertex and the beam axis (< 11 cm) to include most events produced in the decay of a 3% beam halo component. The kaon momentum P_K is computed under the assumptions of the kaon line of flight along the beam axis

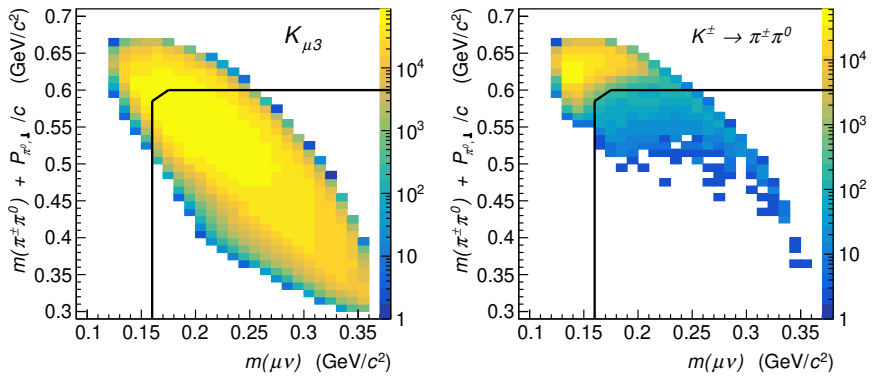

Figure 5. Distributions of the kinematic variables used for $K^{\pm} \to \pi^{\pm}\pi^{0}$ background suppression for MC simulated signal $K^{\pm}_{\mu 3}$ (left) and background $K^{\pm} \to \pi^{\pm}\pi^{0}$ (right) samples. The selection criteria are indicated by solid lines.

and a massless missing neutrino. From the two possible P_K solutions, P_1 and P_2, the one closest to the beam momentum central value is chosen.

The $K^{\pm} \to \pi^{\pm}\pi^{0}\pi^{0}$ ($\pi^{0} \to \gamma\gamma$, $\pi^{0} \to \gamma\gamma$) decays contribute to the background if one of the π^{0} mesons is not detected, and the $\pi^{\pm}$ either decays or is misidentified. This background affects mainly the $K^{\pm}_{\mu 3}$ sample, and is reduced by requiring $|P_1 - P_2| < 60$ GeV/c in this case.

The $K^{\pm} \to \pi^{\pm}\pi^{0}$ background in the $K^{\pm}_{e3}$ sample arising from $\pi^{\pm}$ misidentification is characterized by small total transverse momentum and is reduced by requiring $p_{\nu,\perp} > 30$ MeV/c.

The $K^{\pm} \to \pi^{\pm}\pi^{0}$ background to $K^{\pm}_{\mu 3}$ decays arises from $\pi^{\pm}$ misidentification and $\pi^{\pm} \to \mu^{\pm}\nu$ decay. The former process is suppressed by requiring the $\pi^{0}l^{\pm}$ mass, reconstructed in the π^{+} mass hypothesis for the lepton candidate, to be $m(\pi^{\pm}\pi^{0}) < 0.475$ GeV/c^2, which is below the K^{+} mass considering the resolution of 0.003 GeV/c^2. The latter process is suppressed by requiring the reconstructed $\mu^{\pm}\nu$ invariant mass to be $m(\mu\nu) > 0.16$ GeV/c^2, which is above the π^{+} mass considering the resolution of 0.004 GeV/c^2. Additionally, it is required that $m(\pi^{\pm}\pi^{0}) + p_{\pi^{0},\perp}/c < 0.6$ GeV/c^2, where $p_{\pi^{0},\perp}$ is the π^{0} transverse momentum component with respect to the beam axis. The selection conditions, illustrated in Fig. 5, lead to 17% signal loss and reject 99.5% of the $K^{\pm} \to \pi^{\pm}\pi^{0}$ background.

Samples of 4.4 million K_{e3} (2.3 million $K_{\mu 3}$) events with less than 1 per mille (~2 per mille) background have been selected from the NA48/2 data recorded in 2004 during a four-day long data taking period with reduced beam momentum spread, low intensity and using a minimum bias trigger. Dalitz plots for the both semileptonic modes are shown in the Fig. 6.

Monte Carlo (MC) K_{l3} samples have been simulated using the KLOE generator [13] modified for K_{e3} according to the model-independent (universal) radiative correction proposed in [14]. The concept of universal correction assumes the extraction of effective form factors that absorb all the high-order interplay between the QED and QCD effects. For the $K_{\mu 3}$ mode no considerable disagreement was found between the generator [13] output and the universal radiative correction [14].

The K_{l3} form factor results are obtained by minimization of a χ^2 estimator defined as the sum of contributions $\frac{(D_{i,j}-MC_{i,j})^2}{(\delta D_{i,j})^2+(\delta MC_{i,j})^2}$ over bins(i, j) of the Dalitz plot with at least 20 data

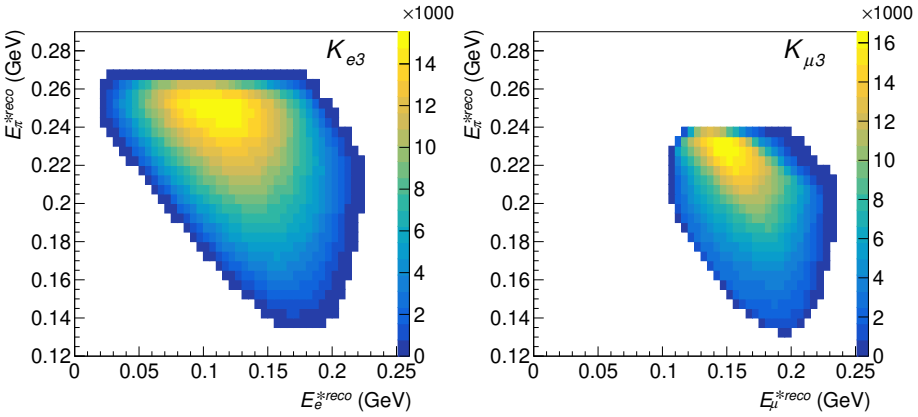

Figure 6. Dalitz plot distributions after the full selection of reconstructed $K^{\pm}_{l3}$ data events. Left: $K^{\pm}_{e3}$ selection, right: $K^{\pm}_{\mu 3}$ selection.

events, where $D_{i,j}$ is the background subtracted number of data events; $MC_{i,j}$ is the number of simulated events in the same bin as obtained from reweighting the MC events for the current iteration parameter values; $\delta D_{i,j}$ and $\delta MC_{i,j}$ are the corresponding errors on $D_{i,j}$ and $MC_{i,j}$. The fit is performed separately for the K_{e3} and $K_{\mu 3}$ Dalitz plots or jointly by extending the summation over both Dalitz plots and using a common set of fit parameters.

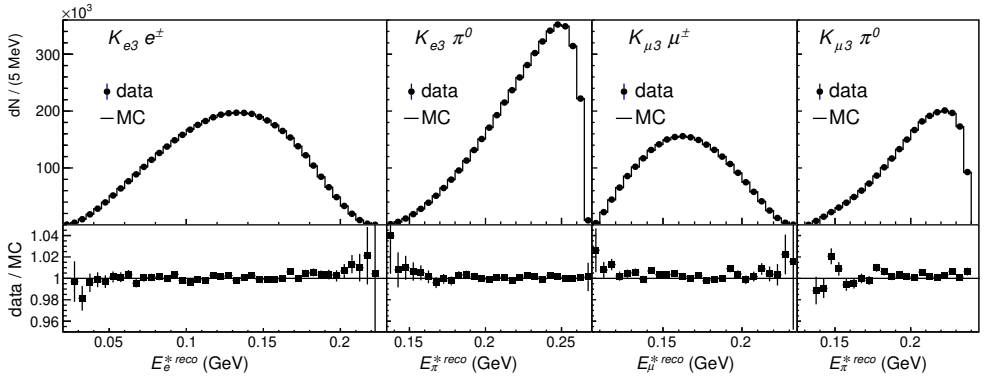

Figure 7. Reconstructed lepton energy E_l^{*reco} and pion energy E_π^{*reco} distributions for $K^{\pm}_{e3}$ and $K^{\pm}_{\mu 3}$ data (after background subtraction) and simulated samples according to the fit results using the Taylor expansion model, and corresponding Data/MC ratios. Simulated distributions according to fit results using other parameterizations cannot be distinguished within the resolution of the plots.

Table 1. Form factor results of the joint $K^{\pm}_{l3}$ analysis. The correlations include both statistical and systematic uncertainties. The units of λ'_+, λ''_+, λ_0, Λ_+ and $\ln C$ values and errors are 10^{-3}. The units of m_V and m_S values and errors are MeV/c^2.

	λ'_+	λ''_+	λ_0	m_V	m_S	Λ_+	$\ln C$
Central values	24.24	1.67	14.47	884.4	1208.3	24.99	183.65
Statistical error	0.75	0.29	0.63	3.1	21.2	0.20	5.92
Diverging beam component	0.97	0.35	0.55	1.1	32.2	0.08	9.43
Kaon momentum spectrum	0.00	0.00	0.02	0.1	0.7	0.00	0.19
Kaon mean momentum	0.04	0.01	0.04	0.2	1.7	0.01	0.47
LKr energy scale	0.66	0.12	0.61	4.9	17.4	0.32	5.16
LKr non-linearity	0.20	0.01	0.55	3.1	19.6	0.20	5.77
Residual background	0.08	0.03	0.04	0.1	0.7	0.01	0.16
Electron identification	0.01	0.01	0.01	0.2	0.2	0.01	0.05
Event pileup	0.23	0.08	0.08	0.4	0.2	0.03	0.07
Acceptance	0.23	0.07	0.03	0.7	4.3	0.05	1.11
Neutrino momentum resolution	0.16	0.04	0.04	0.9	3.3	0.06	0.88
Trigger efficiency	0.29	0.13	0.20	1.1	9.9	0.07	2.82
Dalitz plot binning	0.05	0.04	0.06	0.9	1.1	0.06	0.29
Dalitz plot resolution	0.02	0.01	0.03	0.0	1.3	0.00	0.39
Radiative corrections	0.17	0.01	0.57	2.5	20.1	0.16	5.92
External inputs						0.44	2.94
Systematic error	1.30	0.41	1.17	6.7	47.5	0.62	14.25
Total error	1.50	0.50	1.32	7.4	52.1	0.65	15.43
Correlation coefficient	-0.934 (λ'_+/λ''_+) 0.118 (λ'_+/λ_0) 0.091 (λ''_+/λ_0)			0.374		0.354	
χ^2/NDF	979.6/1070			979.3/1071		979.7/1071	

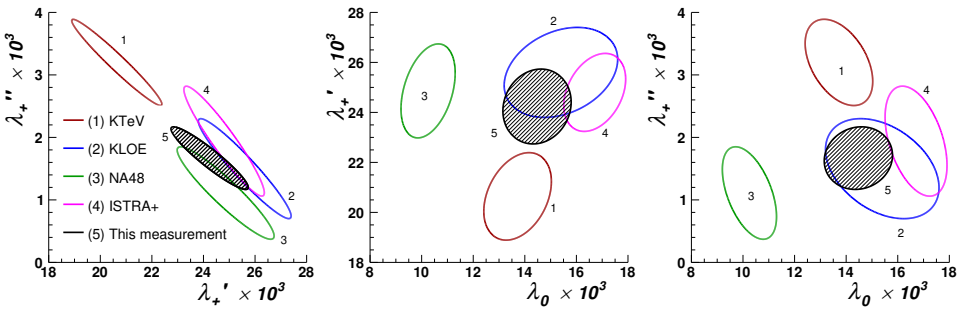

Figure 8. One sigma (39.4% CL) contours for the parameters of the Taylor expansion obtained from the joint analysis together with the combinations of K_{e3} and $K_{\mu 3}$ measurements by the KTeV [15], KLOE [16, 17], NA48 [18, 19], and ISTRA+ [20, 21] Collaborations provided by [22].

Lepton and pion energy projections of the reconstructed Dalitz plots for the data and the simulated samples corresponding to the fit results, along with their ratios Data/MC, are shown in Fig. 7.

The joint K_{l3} analysis form factor results are shown in Table 1 and in the Fig. 8. The systematic errors contributions considered are related to the kaon beam simulation, LKr calibration, background, trigger efficiency, acceptance, radiative correction as well as to the external uncertainty introduced by the extra fixed parameters of the Dispersive parameterization. The measured form factors represent the most precise current result of a combined K_{e3} and $K_{\mu 3}$ analysis.

References

[1] J.R. Batley *et al*, *Eur. Phys. J.* C **52**, 875 (2007)
[2] V. Fanti *et al*, *Nucl. Instrum. Methods* A **574**, 433 (2007)
[3] C. Patrignani *et al* (Particle Data Group), *Chin.Phys.* C **40**, 100001 (2016)
[4] J. Bijnens, G. Ecker, J. Gasser, *Nucl. Phys.* B **396**, 81 (1993)
[5] A.A. Poblaguev *et al*, *Phys. Rev. Lett.* **89**, 061803 (2002)
[6] A.M. Diamant-Berger *et al*, *Physics Letters* B **62**, 485 (1976)
[7] L. Cappiello, O. Cata, G. D'Ambrosio, D. Gao, *Eur. Phys. J.* C **72**, 1872 (2012)
[8] L.M. Chounet, J.M. Gaillard, M.K. Gaillard, *Phys.Rept.* **4**, 199 (1972)
[9] V. Cirigliano *et al*, *Rev. Mod. Phys.* **84**, 399 (2012)
[10] P. Lichard, *Phys. Rev.* D **55**, 5385 (1997)
[11] Batley, J.R. *et al.* (NA48/2 Collaboration), *JHEP* **1810**, 150 (2018)
[12] V. Bernard, M. Oertel, E. Passemar, J. Stern, *Phys. Rev.* D **80**, 034034 (2009)
[13] C. Gatti, *Eur.Phys.J.* C **45**, 417 (2006)
[14] V. Cirigliano, M. Knecht, H. Neufeld, H. Rupertsberger, P. Talavera, *Eur. Phys. J.* C **23** 121 (2002).
[15] T. Alexopoulos *et al.* (KTeV Collaboration), *Phys. Rev.* D **70**, 092007 (2004).
[16] F. Ambrosino *et al.* (KLOE Collaboration), *Phys. Lett.* B **636** 166 (2006).
[17] F. Ambrosino *et al.* (KLOE Collaboration), *JHEP* **0712** 105 (2007).
[18] A. Lai *et al.* (NA48 Collaboration), *Phys. Lett.* B **604** 1 (2004).
[19] A. Lai *et al.* (NA48 Collaboration), *Phys. Lett.* B **647** 341 (2007).
[20] O. Yushchenko *et al.*, (ISTRA+ Collaboration), *Phys. Lett.* B **581** 31 (2004).
[21] O. Yushchenko *et al.*, (ISTRA+ Collaboration), *Phys. Lett.* B **589** 111 (2004).
[22] M. Antonelli *et al.* (FlaviaNet Working Group on Kaon Decays), *Eur. Phys. J.* C **69** 399 (2010).